Research paper

Using iron speciation in authigenic carbonates from hydrocarbon seeps to trace variable redox conditions

Yu Hu [a, e], Dong Feng [b, *], Linying Chen [b], Guodong Zheng [c], Jörn Peckmann [d], Duofu Chen [a, *]

[a] CAS Key Laboratory of Marginal Sea Geology, Guangzhou Institute of Geochemistry, Chinese Academy of Sciences, Guangzhou 510640, China
[b] CAS Key Laboratory of Marginal Sea Geology, South China Sea Institute of Oceanology, Chinese Academy of Sciences, Guangzhou 510301, China
[c] Key Laboratory of Petroleum Resources, Gansu Province/Key Laboratory of Petroleum Resources Research, Institute of Geology and Geophysics, Chinese Academy of Sciences, Lanzhou 730000, China
[d] Department of Geodynamics and Sedimentology, Center for Earth Sciences, University of Vienna, 1090 Vienna, Austria
[e] University of Chinese Academy of Sciences, Beijing 100049, China

ABSTRACT

Seepage of hydrocarbon-rich fluids out of the marine sedimentary column is characterized by temporal changes of flow intensity and resultant spatially variable redox conditions. Authigenic carbonates at marine hydrocarbon seeps provide excellent geological and geochemical archives that serve to explore seepage dynamics over time. In this study, we investigated the potential of Mössbuaer spectroscopy and Fe contents of seep-related authigenic carbonates from the Congo Fan, the Gulf of Mexico, and the Black Sea for reconstructing past redox conditions and fluid seepage activity at cold seeps. The Fe speciation observed by Mössbauer spectroscopy and Fe contents suggest that (1) the Congo Fan carbonates precipitated in a sulfidic environment, (2) the formation conditions of seep carbonates were variable at the Gulf of Mexico seep site, ranging from oxic to suboxic and anoxic and even spanning into the methanogenic zone, and (3) the stratified water column of the Black Sea or suboxic condition resulted in low Fe contents of Black Sea carbonates. The study reveals that Fe speciation can provide constraints on the wide range of redox conditions that imprinted seep carbonates during the life span of seepage. Similarly, Mössbauer spectroscopy — particularly when used in combination with the analysis of redox-sensitive elements — is a promising tool to trace variable redox conditions in marine paleoenvironments other than seeps.

© 2015 Elsevier Ltd. All rights reserved.

1. Introduction

Seepage of cold hydrocarbon-rich fluids is a widely observed phenomenon in the marine sedimentary strata along continental margins (e.g. Campbell, 2006; Peckmann and Thiel, 2004; Suess, 2014, and many others). The key biogeochemical process at seeps is the anaerobic oxidation of methane (AOM) coupled with the sulfate reduction (Boetius et al., 2000; Boetius and Wenzhöfer, 2013), which results in the precipitation of authigenic carbonates and iron sulfides close to the seafloor (Berner, 1980). Iron-bearing minerals (e.g. pyrite, siderite, ankerite) are among the diagenetic products of this process, and are frequently observed in association

with the predominant calcium carbonate minerals at seeps (e.g. Chen et al., 2006; Dewangan et al., 2013; González et al., 2012; Peckmann et al., 2001; Sun et al., 2015; Zhang et al., 2014). Numerous seafloor observations revealed significant variability of chemical and physical parameters and associated early diagenetic conditions within shallow subsurface sediments at seeps (e.g. Greinert, 2008; Macelloni et al., 2013; Schneider von Deimling et al., 2011; Solomon et al., 2008; Tyron et al., 1999; Tyron and Brown, 2004). Such variability is usually reflected in complex geochemical signatures of authigenic seep carbonates (e.g. Bohrmann et al., 1998; Feng et al., 2013, 2009; Greinert et al., 2001; Han et al., 2014; Liebetrau et al., 2014; Peckmann et al., 2001; Peckmann and Thiel, 2004; Suess, 2014). For example, some redox-sensitive elements and rare earth elements, mostly using molybdenum (Mo)−uranium (U) covariation and cerium (Ce) anomalies, have been used to trace redox variations during the

---

formation of seep carbonates (e.g. Feng et al., 2013, 2009; Ge et al., 2010; Himmler et al., 2010; Hu et al., 2014; Rongemaille et al., 2011). These studies helped to constrain the paleo-redox condition at seeps and allowed to trace past fluid flow and associated environmental changes at a regional scale (e.g. Bayon et al., 2013; Crémière et al., 2013). However, given the uncertainties of this proxy-based approach, it is somewhat difficult to constrain redox variations with an only limited number of measures, using Ce anomalies and Mo-U covariation, as outlined by Himmler et al. (2010)and Hu et al. (2014).

Because (1) iron (Fe) is much more mobile in seawater or pore fluid in the absence of molecular oxygen and hydrogen sulfide, and because of (2) effective retention of Fe under sulfidic or oxygenated conditions in the sediment (e.g. Lyons and Severmann, 2006; Owens et al., 2012; Raiswell and Canfield, 2012; Severmann et al., 2010; Scholz et al., 2014a,b), Fe is a potential redox proxy that allows constraining the formation conditions of marine sediments and sedimentary rocks. Studies on Fe in sediments at seeps and in authigenic seep deposits mainly focused on the geochemical cycling of Fe and the involved biogeochemical processes (Bayon et al., 2011; Beal et al., 2009; González et al., 2012; Lemaitre et al., 2014; Pierre et al., 2014; Riedinger et al., 2014; Sivan et al., 2014; Sun et al., 2015; Zhang et al., 2014). In particular, Fe oxides can stimulate sulfate-driven AOM at seeps (Beal et al., 2009; Sivan et al., 2014). Iron sometimes plays a critical role in biogeochemical processes at seeps, leading occasionally to the formation of orange iron-oxidizing microbial mats on the seafloor (Omoregie et al., 2008). High Fe concentrations are frequently found in methane plumes (Bayon et al., 2011; Charlou et al., 2004; Lemaitre et al., 2014) and this process could lead to the precipitation of Fe-oxyhydroxide and/or nanosulfide phases as well (Lemaitre et al., 2014). So far, Fe geochemistry has not been used to trace the variability of redox conditions and the formation environment of authigenic minerals at seeps.

Mössbauer spectroscopy is among the most advanced methods to determine Fe species and their relative contents in iron-bearing materials, including Fe^{3+}/Fe^{2+} ratios (e.g. Medina et al., 2006; Peiffer et al., 2015; Ram et al., 1998; Vandenberghe and Grave, 2013; Zachara et al., 2004; Zhang et al., 2013; Zheng et al., 2010, 2002). These parameters related to Fe contents and speciation are effective tools for the analysis of redox conditions (e.g. Zheng et al., 2010, 2002). Here, we performed ^{57}Fe Mössbauer spectroscopy on authigenic carbonates from five modern seeps of three locations, the Congo Fan, the Gulf of Mexico and the Black Sea. Mössbauer spectroscopy was underpinned by the analysis of major and trace elements. Iron speciation obtained by Mössbauer spectroscopy was then used to examine its potential as a paleo-redox indicator at seeps, allowing to constrain the formation conditions of seep carbonates and to trace past changes of redox conditions as well.

2. Background information: Iron as an effective redox proxy in marine sediments and sedimentary rocks

As one of the most common and widely distributed redox-sensitive element in the environment, Fe has been widely used to illustrate the redox states and processes of modern and ancient marine environments (e.g. Lyons and Severmann, 2006; Owens et al., 2012; Raiswell and Canfield, 2012; Scholz et al., 2014a,b; Tribovillard et al., 2015). Due to the thermodynamical stability of Fe^{3+} in oxygenated environments, oxygenated marine surface sediment receive and retain ferric Fe with a very low sedimentary Fe export flux (Scholz et al., 2014a,b). This circumstance is reflected in relatively high contents of authigenic Fe in marine sediments (Fig. 4a; Scholz et al., 2014a,b). Under suboxic to anoxic conditions and ferruginous conditions prevailing, on the other hand, Fe export in the dissolved state from surface sediment is favored, resulting in Fe pauperized sediments (Fig. 4a; Severmann et al., 2010; Scholz et al., 2014a,b). Under such oxic/suboxic conditions in marine
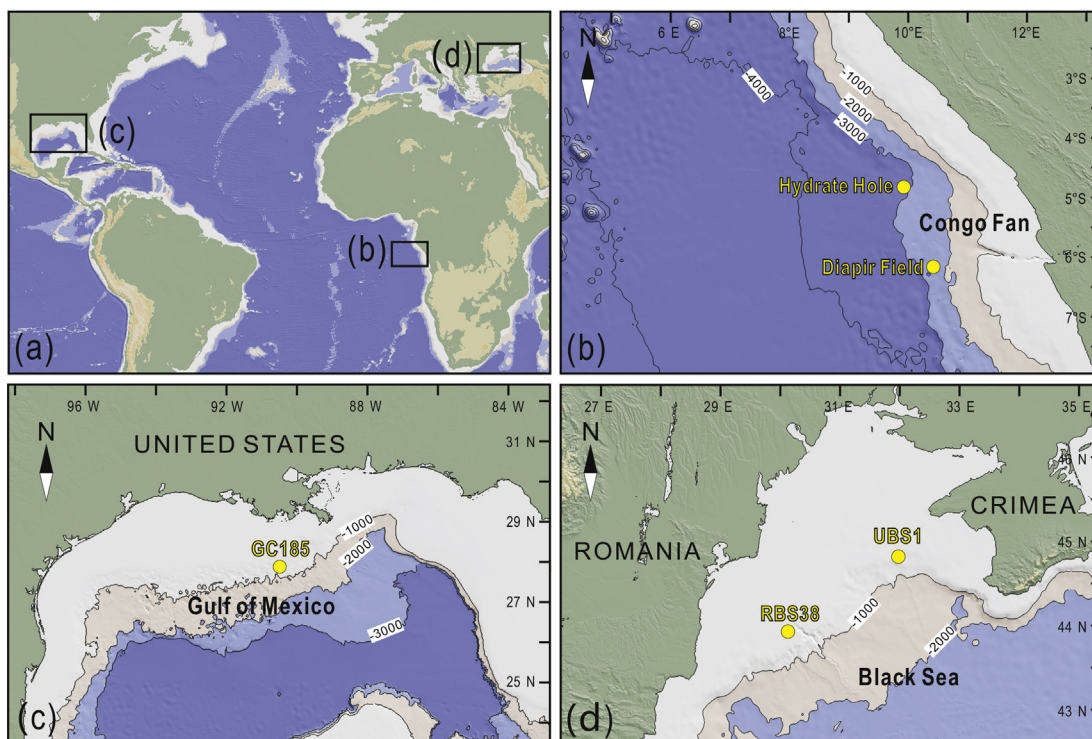

Figure 1. Global map (a) showing the study areas, (b) Congo Fan, (c) Gulf of Mexico, and (d) Black Sea. Maps (b) to (d) contain bathymetric information.
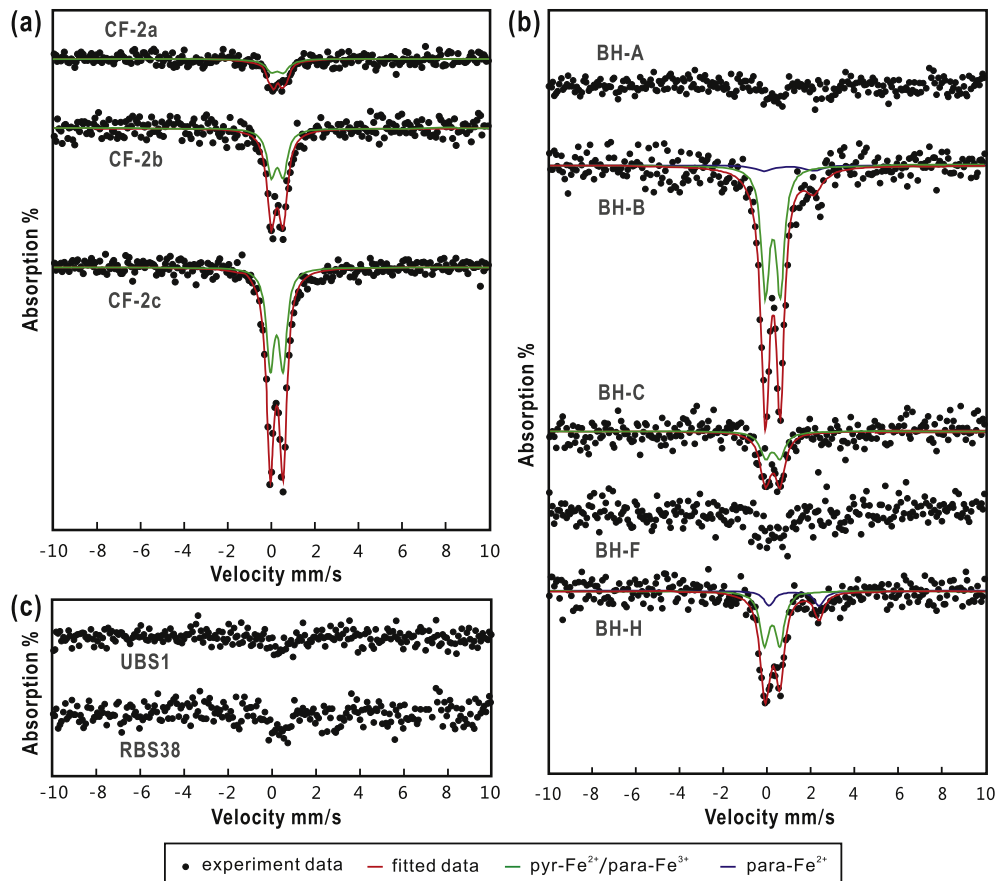
Figure 2. Typical ^{57}Fe Mössbauer spectra and fitting results of seep carbonates from (a) the Congo Fan, (b) the Gulf of Mexico, and (c) the Black Sea.

environment, Fe biogeochemical cycling is closely related to pre-cipitation/dissolution of Fe-oxyhydroxides (Froelich et al., 1979; Thomson et al., 1993). As Fe-oxyhydroxides in oxic zone are further buried into suboxic condition, they experience reductive dissolution and release reduced Fe into pore water. The diffusion and/or advection of reduced Fe pore water towards the seafloor leads to re-precipitation and enrichment of Fe-oxyhydroxides in near-surface sediments (Froelich et al., 1979; Lemaitre et al., 2014; Thomson et al., 1993). Finally, in surface sediments affected by

sulfidic conditions, most of the ferrous Fe is retained as iron sul-fides, preventing Fe export out of the near-surface sediments and favoring authigenic Fe accumulation (Fig. 4a; Raiswell and Canfield, 2012; Scholz et al., 2014a,b). Geochemical cycling of Fe caused by variable redox conditions is most pronounced in the seawater column and within the uppermost sediment horizons. Still, similar processes also occur in diagenetic pore fluids with authigenic mineral formation deeper in the sediment (Raiswell and Canfield, 2012). Namely, cycling of Fe is also pronounced in the methano-genic zone, which is particularly common on continental margins (e.g. Hensen et al., 2003; Joye et al., 2009, 2005; März et al., 2008; Riedinger et al., 2014). The methanogenic zone is often particularly prominent in the surface sediment affected by seepage, where sulfate consumption pushes this zone to relatively shallow horizons (cf. Joye et al., 2009, 2005; Riedinger et al., 2014). In such envi-ronments, high concentrations of ferrous Fe are present in the pore fluids (Hensen et al., 2003; Joye et al., 2009, 2005; Riedinger et al., 2014). This ferrous Fe either diffuses into the sulfidic zone to form iron sulfides (Hensen et al., 2003; Riedinger et al., 2014) or is locally incorporated into carbonate minerals that form if alkalinity is high enough to allow for the precipitation of Ca and Fe carbonates (Fig. 4a; González et al., 2012; Malone et al., 2002; Pierre et al., 2014). Therefore, the behavior of Fe varies in different redox zones, which, in turn, can be used as an effective redox proxy for marine sediments and ancient sedimentary rocks.

3. Materials and methods

Authigenic carbonates from five seep sites of the Congo Fan, the Gulf of Mexico and Black Sea were chosen in this study (Fig. 1). All
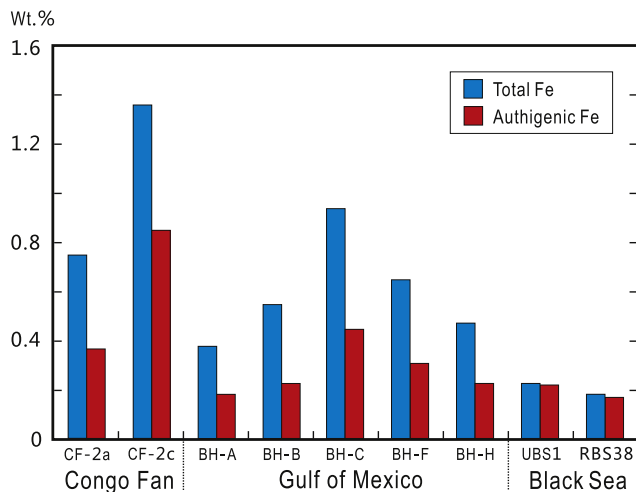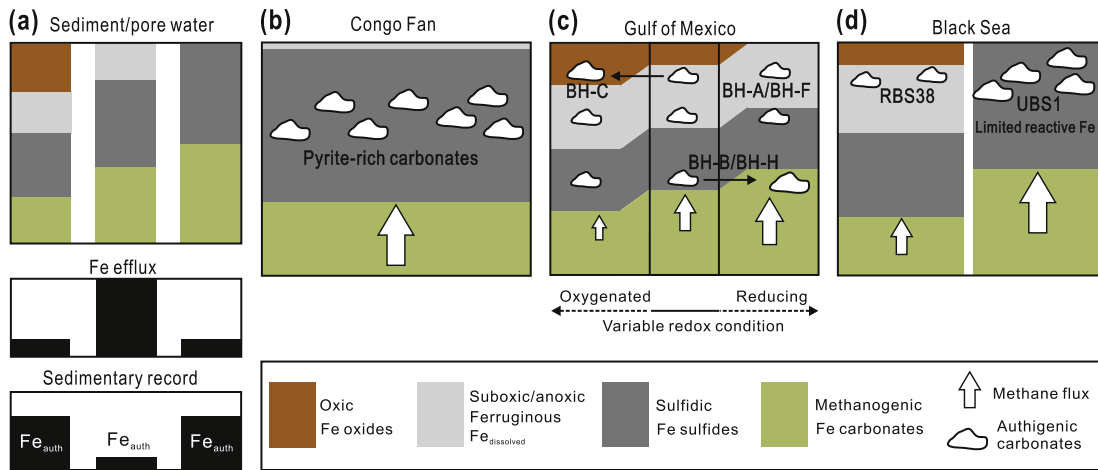

Figure 3. Relative weight percentages (wt.%) of total Fe and authigenic Fe of seep carbonates from the Congo Fan, the Gulf of Mexico, and the Black Sea.

Figure 4. Schematic diagram illustrating the different state of Fe in pore water and sediment that changes as a function of redox conditions and various formation environments of seep carbonates. (a) Variable redox conditions resulting in the different state of Fe and associated paleo-proxy retained in marine sediment (modified from Scholz et al., 2014a). (b) The sulfidic formation condition of the Congo Fan seep carbonates. (c) Variable redox conditions during formation of the Gulf of Mexico seep carbonates. The primary formation environment of seep carbonates is sulfidic or suboxic/anoxic, allowing for the anaerobic oxidation of methane to take place. As the conditions become more reducing or oxygenated as a function of variable methane fluxes, seep carbonates may subsequently be altered in the methanogenic zone (samples BH-B and BH-H) upon increased seepage or in the oxic zone (sample BH-C) upon sluggish flow, respectively. (d) The suboxic conditions (RBS38) or a euxinic water column (UBS1), resulting in limited reactive Fe in the sediment, are suggested to explain the low Fe content in the Black Sea seep carbonates. Arrow sizes are proportional to upward methane fluxes.

carbonates have been shown to represent marine hydrocarbon-seep deposits (Hass et al., 2010; Feng et al., 2010, 2009; Peckmann et al., 2001). The Congo Fan carbonates analyzed here were collected by TV-guided grabs from the sites Hydrate Hole and Diapir Field during RV METEOR Cruise M56. The GC185 carbonates from the Gulf of Mexico were collected at the Bush Hill site during the Johnson-Sea-Link I (JSL I) manned submersible dives in 1997 and 1998. The Black Sea samples were collected during R/V Professor Vodyanitskiy (1993, and 1994) and R/V Poseidon (1994) cruises. Location, water depth, morphology, $\delta^{13}C_{carbonate}$ values, mineralogy, and the cerium (Ce) anomalies of the carbonate samples are listed in Table 1.

The carbonate samples were grounded to 100-mesh powder using an agate mortar and pestle. For ^{57}Fe Mössbauer spectroscopy, about 300 mg powder samples without any chemical pretreatment were transferred into a brass sample holder (16 mm in diameter, 1 mm thick). The Mössbauer spectra were measured by an Austin Science S-600 Mössbauer spectrometer using a γ-ray source of 1.11 GBq ^{57}Co/Rh at room temperature (293 K) at Lanzhou Center for Oil and Gas Resources, Chinese Academy of Sciences. Isomer shifts were expressed according to the centroid of the spectrum of

metallic Fe foil. The obtained Mössbauer spectra were fitted to Lorentzian lineshapes using standard line-shape fitting routines. The intensity and half width of quadruple doublet peaks were adjusted to be equal.

Powdered samples for major and trace element analysis of bulk carbonates were placed in Teflon beakers, and dissolved by mixture of 1 ml of HF and 1 ml of HNO$_3$. The method used for the chemical treatment procedure was the same as that described in Hu et al. (2014). The elemental analyses were performed using a Varian Vista Pro ICP-AES for major elements and a Perkin−Elmer Sciex ELAN 6000 ICP-MS for trace elements. All samples were analyzed at the Institute of Geochemistry, Chinese Academy of Sciences. Certified reference materials (GSR-12, GSR-13, OU-6, AMH-1 and GBPG-1) were used for quality control. Precision and accuracy were better than 5% for major elements and Sr. Only the authigenic fraction of elements can be used for paleoenvironmental indicators (Scholz et al., 2014a; Tribovillard et al., 2015, 2006). The authigenic fraction corresponds to the Fe content in excess of the calculated lithogenic fraction. Consequently, the authigenic fraction of element X in a sample can be calculated by $X_{auth} = (X)_{sample} − Al_{sample} \times (Fe/Al)_{lithogenic}$ (Scholz et al., 2014a; Tribovillard et al., 2015, 2006). The

Table 1
Location, water depth, morphology, $\delta^{13}C_{carbonate}$ values, mineralogy, and cerium anomalies of the seep carbonates.

| Sample ID | Water depth (m) | Morphology of carbonates | δ^{13}C (‰ VPDB) | Relative percentages of mineral composition by XRD (wt. %) | | | | | | | Ce/Ce* | References |
				Ara	Cc	Dol	Bar	Kao	Ms	Qz		
Congo Fan												
CF-2a	3117	nodules, crusts, and slabs,	−62.5 to −46.3	89.6	2.6	−	3.1	4.6	−	−	1.54−1.84	Feng et al., 2010;
CF-2b	3117	tubes, and filled molds		17.0	74.3	−	−	5.3	−	3.4	1.56−1.62	Hu et al., 2014
CF-2c	2417	nodules, crusts, and slabs	−40.7 to −30.7	68.1	29.6	−	−	1.3	−	1.0	1.25−1.27	
Gulf of Mexico												
BH-A	540	Slabs and blocks	−29.4 to −19.7	94.9	5.1	−	−	−	<0.1	−	0.79−0.87	Feng et al., 2009
BH-B			−24.2	88.5	3.8	−	−	1.7	4.8	−	0.92	
BH-C			−20.1 to −5.0	99.0	0.9	−	−	−	0.1	−	0.40−0.46	
BH-F			−27.9 to −22.8	97.1	2.9	−	−	−	−	−	0.89−0.97	
BH-H			−17.9 to −4.1	88.7	3.3	7.8	−	−	−	−	0.99	
Black Sea												
UBS1	190	crusts	−41.0 to −25.9	48.6	51.4	−	−	−	−	−	0.88−0.99	Feng et al., 2013
RBS38	120	crusts	−37.3 to −28.9	22.1	77.9	−	−	−	−	−	0.61−0.79	

Ara = aragonite, Cc = calcite, Dol = dolomite, Bar = barite, Kao = kaolinite, Ms = Muscovite, Qz = quartz, Ce/Ce* = cerium anomaly.

Table 2
Mössbauer parameters of the iron compounds in the seep carbonates.

Sample ID	Total peak area/% mm s^{-1}	Iron species	Relative content %	IS/mm s^{-1}	QS/mm s^{-1}	HW/mm s^{-1}
Congo Fan						
CF-2a	0.16 ± 0.01	Pyr-Fe^{2+}/para-Fe^{3+}	100	0.349 ± 0.026	0.550 ± 0.042	0.299 ± 0.036
CF-2b	0.48 ± 0.01	Pyr-Fe^{2+}/para-Fe^{3+}	100	0.338 ± 0.009	0.535 ± 0.019	0.247 ± 0.013
CF-2c	0.93 ± 0.01	Pyr-Fe^{2+}/para-Fe^{3+}	100	0.312 ± 0.003	0.580 ± 0.005	0.218 ± 0.004
Gulf of Mexico						
BH-A	n.d.					
BH-B	0.72 ± 0.02	Pyr-Fe^{2+}/para-Fe^{3+}	82.47	0.339 ± 0.007	0.684 ± 0.013	0.222 ± 0.007
		para-Fe^{2+}	17.53	1.070 ± 0.108	2.302 ± 0.198	0.482 ± 0.135
BH-C	0.17 ± 0.01	Pyr-Fe^{2+}/para-Fe^{3+}	100	0.331 ± 0.023	0.665 ± 0.040	0.287 ± 0.041
BH-F	n.d.					
BH-H	0.33 ± 0.01	Pyr-Fe^{2+}/para-Fe^{3+}	74.15	0.313 ± 0.007	0.708 ± 0.013	0.251 ± 0.031
		para-Fe^{2+}	25.85	1.313 ± 0.052	2.295 ± 0.104	0.275 ± 0.072
Black Sea						
UBS1	n.d.					
RBS38	n.d.					

n.d.: not detected. IS: isomer shifts; QS: quadruple splitting; HW: half width of quadruple doublet peaks.

average composition of the upper crust (McLennan, 2001) was chosen as the lithogenic background.

4. Results

4.1. Mössbauer spectroscopy

The Mössbauer spectra of the authigenic carbonates are shown in Figure 2 and the Mössbauer parameters are given in Table 2. All doublets in the Mössbauer spectra are regarded to be symmetric here. All the Congo Fan carbonates have one doublet peak, but the Black Sea carbonates have apparently little Fe, as their spectra exhibited no clear absorption peaks, which indicates that the Fe concentrations of these samples are below the detection limit determined of Mössbauer spectroscopy. The Gulf of Mexico carbonates have quite different spectra among each other, showing no clear absorption peaks (BH-A and BH-F), one doublet peak (BH-C), and two doublet peaks (BH-B and BH-H). According to the obtained Mössbauer parameters, the doublets in Congo Fan carbonates have smaller isomer shifts and quadruple splitting resulting from either paramagnetic high-spin ferric Fe (para-Fe^{3+}) or Fe in pyrite (pyr-Fe^{2+}). The para-Fe^{3+} probably originated from hydrated Fe(III) oxides and/or clay minerals (cf. Zheng et al., 2010). Although the similar range of isomer shifts and quadruple splitting make it difficult to identify pyrite among Fe^{3+}-containing clay minerals

(e.g. Vandenberghe and Grave, 2013; Zheng et al., 2010), hyperfine parameter values of Congo Fan carbonates are much closer to that of pyrite (Isomer shifts = 0.31 mm/s; Quadruple splitting = 0.61 mm/s), which is best explained by its presence in the studied samples. In addition, there is a gradual increase in total peak area and decrease in isomer shifts and half width among samples CF-2a, CF-2b and CF-2c (Table 2). The doublets of Gulf of Mexico carbonates with smaller isomer shifts and quadruple splitting (BH-B, BH-C, and BH-H) are attributable to either para-Fe^{3+} or pyr-Fe^{2+} (Table 2), while carbonate samples (BH-B and BH-H) exhibiting larger isomer shifts and quadruple splitting correspond to paramagnetic ferrous Fe (para-Fe^{2+}).

4.2. Major and trace elements

Selected major and trace element contents are present in Table 3. The comparison of the element contents of the seep carbonates with that of the upper crust (McLennan, 2001) indicates a minor contribution of lithogenic components for some of the elements (e.g. Ca, Mg, Sr), while a considerable contribution of lithogenic iron-bearing minerals is apparent (Table 3). All studied rock samples have high carbonate contents ranging from ~78 wt.% to ~91 wt.%. High manganese contents were only observed in BH-C and Black Sea carbonate samples. The Congo Fan carbonates exhibit higher total Fe (Fe$_T$) and authigenic Fe (Fe$_{auth}$) contents than

Table 3
Selected major and trace element concentrations, and calculated carbonate and authigenic Fe contents of the seep carbonates.

Sample ID	Ca wt %	Mg wt %	Al wt %	Sr ppm	Mn wt %	Fe$_T$[a] wt %	CaCO$_3$ wt %	MgCO$_3$ wt %	SrCO$_3$ wt %	$\sum$Carb[b] wt %	Fe$_{auth}$[c] wt %
Congo Fan											
CF-2a	30.5	1.62	0.88	7430	0.01	0.75	76.3	5.7	1.25	83.3	0.37
CF-2b	–	–	–	–	–	–	–	–	–	–	–
CF-2c	28.8	1.60	1.17	4730	0.02	1.36	72.0	5.6	0.80	78.4	0.85
Gulf of Mexico											
BH-A	30.2	1.85	0.45	5710	0.01	0.38	75.4	6.5	0.96	82.9	0.18
BH-B	30.9	0.85	0.74	6790	0.02	0.55	77.2	3.0	1.14	81.3	0.23
BH-C	30.3	0.44	1.12	7620	0.11	0.94	75.9	1.5	1.28	78.7	0.45
BH-F	31.1	0.93	0.78	6450	0.01	0.65	77.9	3.2	1.09	82.2	0.31
BH-H	32.6	0.73	0.55	7700	0.01	0.47	81.6	2.5	1.30	84.4	0.23
Black Sea											
UBS1	34.4	0.84	0.02	5910	0.10	0.23	85.9	2.9	1.00	89.8	0.22
RBS38	33.2	2.11	0.01	1070	0.50	0.18	83.0	7.4	0.18	90.6	0.17
Upper Crust[d]	3.00	1.33	8.04	350	0.06	3.50	–	–	–	–	–

[a] Fe$_T$ = Total Fe.
[b] $\sum$Carb = CaCO$_3$ + MgCO$_3$ + SrCO$_3$.
[c] Fe$_{auth}$ = authigenic Fe, calculated by Fe$_{auth}$ = (Fe$_T$)$_{sample}$ − Al$_{sample}$ × (Fe/Al)$_{Upper\ Crust}$.
[d] Data from McLennan (2001).

the Black Sea carbonates. The Gulf of Mexico carbonates revealed variable Fe_T and Fe_{auth} contents with relatively higher ones in BH-C and lower ones in BH-A (Table 3; Fig. 3).

5. Discussion

5.1. The formation conditions of seep carbonates constrained by iron speciation

5.1.1. Seep carbonates of the Congo Fan

The Congo Fan carbonates are mainly composed of aragonite and high-Mg calcite, associated with abundant pyrite framboids (Feng et al., 2010; Haas et al., 2010; Pierre and Fouquet, 2007). The extremely negative $\delta^{13}C$ values of the authigenic carbonates indicate that the carbon was derived from oxidation of biogenic methane (Feng et al., 2010; Haas et al., 2010; Pierre and Fouquet, 2007). The isomer shifts and quadruple splitting values of Congo Fan carbonates are close to those of pyrite, suggesting that the authigenic Fe in the carbonates is indeed mainly represented by pyrite. This inference is consistent with the relatively high Fe_T and Fe_{auth} contents and the observation of abundant pyrite by optical microscopy (cf. Feng et al., 2010; Haas et al., 2010; Pierre and Fouquet, 2007). According to the well documented behavior of Fe in marine sediments, the high content of authigenic Fe mainly represented by pyrite suggests that sulfidic conditions prevailed during formation of the Congo Fan carbonates (Fig. 4b). Such sulfidic conditions are also supported by positive Ce anomalies, high Mo contents, and high $(Mo/U)_{auth}$ ratios (Hu et al., 2014). In addition, the gradual increase in the total peak area and decrease in isomer shifts and quadruple splitting from subsample CF-2a over CF-2b to CF-2c is best explained by an increasing degree of pyritization.

5.1.2. Seep carbonates of the Gulf of Mexico

The major mineral in the Gulf of Mexico carbonates is aragonite, with minor amounts of calcite and dolomite (Feng et al., 2009). The $\delta^{13}C$ values of the Gulf of Mexico carbonates range from $-29.4‰$ to $-4.1‰$ (Table 1). The moderately negative $\delta^{13}C$ values have been interpreted to suggest that the carbon predominantly derived from microbial degradation of crude oil (Feng et al., 2009). Moreover, the highest $\delta^{13}C$ values have been suggested to reflect admixture of carbon from a ^{13}C-enriched dissolved inorganic source, either seawater or pore fluids of the methanogenic zone (cf. Feng et al., 2009; Peckmann and Thiel, 2004; Pierre et al., 2014; Roberts and Aharon, 1994).

The Mössbauer parameters of the samples BH-B and BH-H show a wide range of isomer shifts and quadruple splitting (Table 2). The smaller isomer shifts and quadruple splitting are attributable to either para-Fe^{3+} or pyr-Fe^{2+}. The larger isomer shifts and quadruple splitting correspond to para-Fe^{2+}, which can be contributed to ferrous Fe in clay minerals (e.g. kaolinite and muscovite in BH-B and BH-H) or iron-bearing carbonates (e.g. siderite and ankerite). The latter is more likely due to the very similar isomer shifts and quadruple splitting to that of siderite (cf. Medina et al., 2006; Ram et al., 1998; Zachara et al., 2004; Zheng et al., 2010). Additionally, kaolinite and muscovite tend to contain little Fe (Vandenberghe and Grave, 2013). Thus, accessory siderite or possibly ankerite rather than clay minerals have apparently caused the Mössbauer patterns, reflecting abundant ferrous Fe. We unfortunately failed to detect Fe carbonate minerals in BH-B and BH-H samples by XRD analysis, probably because of their low contents that below the detection limit. Still, the combined evidence suggests that the formation conditions of the BH-B and BH-H samples were affected by methanogenesis (Fig. 4c). As a note of caution it is stressed that sulfidic formation conditions cannot be excluded if the smaller isomer shifts and quadruple splitting would be attributed to pyr-Fe^{2+}. Nonetheless, the formation environment was strongly reducing, agreeing well with the absence of negative Ce anomalies in the BH-B and BH-H carbonates (Table 1).

Relatively high contents of Fe_T and Fe_{auth} were observed for BH-C carbonate sample (Table 3; Fig. 3). Its Mössbauer parameters reveal smaller isomer shifts and quadruple splitting, resulting from either para-Fe^{3+} or pyr-Fe^{2+} (Table 2; Fig. 2). Considering the strongly negative Ce anomalies observed in subsamples of BH-C, the formation of BH-C carbonate was apparently at least episodically affected by oxic conditions (Fig. 4c). More oxidizing conditions best explain the relatively higher Fe_{auth} content and the Mössbauer parameters (para-Fe^{3+} in this case). The Mössbauer spectra of BH-A and BH-F samples revealed no clear absorption peaks (Fig. 2). The lack of distinct peaks was probably caused by a too low Fe content that below the detection limit (cf. Zhang et al., 2013), which is consistent with the lower Fe_{auth} content than sample BH-C. Taken together, these arguments suggest that BH-A and BH-F carbonates formed in a suboxic environment, which favored the loss of Fe to the water column. Such inferred suboxic conditions agree with the slightly negative Ce anomalies observed in BH-A and BH-F carbonates (Table 1).

It may seem surprising at first glance that carbonate formation occurred in very different redox environments at one seep site. However, moving redox fronts have been reported for modern seeps and are believed to be governed by variations in methane flux (Chen et al., 2004; Solomon et al., 2008; Tryon et al., 1999; Tryon and Brown, 2004). Such environmental variability has also been found to be archived in redox-sensitive geochemical proxies in seep carbonates (e.g. Birgel et al., 2011; Feng et al., 2013). The variable redox conditions for the Gulf of Mexico carbonates are also supported by the variable Ce anomalies and the complex carbon source of the ^{13}C isotope (Table 1; Feng et al., 2009).

5.1.3. Seep carbonates of the Black Sea

The minerals in the Black Sea seep deposits are mainly aragonite and high-Mg calcite with little clay minerals incorporated into the matrix (Table 1; Peckmann et al., 2001). The RBS38 carbonates were collected at 120 m water depth with oxygen concentration of 11 μmol/L, and UBS1 carbonates at 190 m water depth with high hydrogen sulfide concentration of 140 μmol/L (Peckmann et al., 2001). Although framboidal pyrite and greigite were reported in some of the seep carbonates (Peckmann et al., 2001; Reitner et al., 2005), the Black Sea carbonates studied here have little Fe based on no clear absorption peaks of the Mössbauer spectra and low contents of Fe_T and Fe_{auth}. Similar patterns with low contents of Fe and aluminosilicates were also reported for seep carbonates from the Crimean Slope of the Black Sea (Novikova et al., 2015). The little Fe and slightly negative Ce anomalies in RBS38 carbonates agree with suboxic formation conditions (Fig. 4d). However, such suboxic conditions can be excluded for the formation environment of the UBS1 carbonates with the high hydrogen sulfide concentrations of the bottom water at 190 m water depth. The UBS1 carbonates revealed not only a low Fe content but also a low aluminum content (Table 3). One reason for the low Fe content of the UBS1 carbonate is that the sample contains little aluminosilicates (e.g. clay minerals). Moreover, the circumstance that the dominant control on pyrite formation under euxinic conditions is the availability of reactive Fe in the detrital fraction typically results in Fe-limited pyrite formation in the Black Sea (Berner, 1984; Calvert and Karlin, 1991; Lyons and Berner, 1992; Raiswell and Canfield, 2012). Despite of the sulfidic formation conditions of the UBS1 carbonates, the limited reactive Fe in the local sedimentary environment apparently prevented pronounced pyrite formation

(Fig. 4d), resulting in low Fe accumulation in the authigenic carbonates.

5.2. The applicability of iron speciation as a proxy for redox conditions at seeps − an outlook

Overall, Mössbauer spectroscopy complemented by the analysis of Fe contents is an effective approach to determine Fe speciation and to recognize Fe-bearing minerals, which allows to constrain the redox conditions during the formation of authigenic mineral phases at seeps. As revealed by previous work, Ce anomalies can be used to distinguish between oxic and anoxic conditions, although it is difficult to exclude the possibilities that high alkalinity and organic-rich pore fluids may compromise the validity of Ce anomalies (e.g. Hu et al., 2014; Kim et al., 2012). The Mo-U covariation is a proxy that is commonly used to distinguish conditions ranging from sulfidic to suboxic (e.g. Algeo and Tribovillard, 2009; Hu et al., 2014). However, the Ce and Mo-U redox proxies do not allow to identify the whole range of redox conditions that typify marine sediments ranging from oxic over suboxic-anoxic and sulfidic to methanogenic. Iron speciation used here as a redox proxy to constrain the conditions during mineral authigenesis at seeps has potential to overcome this limitation − particularly when applied in combination with other redox proxies. It needs to be stressed that some factors (e.g. low Fe content, high clay minerals content) may hamper the recognition of Fe speciation by Mössbauer spectroscopy analysis, which limits the applicability of Fe speciation in the endeavor of constraining redox conditions. In addition, the presence of Fe-oxyhydroxides in carbonates may complicate the interpretation of Mössbauer spectroscopy data. Seep-related carbonates on the seafloor are usually coated with a thin layer of Fe-oxyhydroxides (e.g. Bayon et al., 2013). Such Fe-oxyhydroxide coatings may be related to precipitation of hydrogenous Fe−Mn oxides, and also to oxidation of reduced Fe-rich fluids that are expelled into bottom waters at seeps (Lemaitre et al., 2014). Consequently, some of the observed variation in Mössbauer spectroscopy data might reflect the presence of variable amounts of Fe-oxyhydroxides rather than changes in redox processes. Therefore, careful sample preparation, e.g. removal of Fe-oxyhydroxides coatings before analysis, is critical to obtain reliable Mössbauer spectroscopy data. Despite these drawbacks, Fe speciation as an effective redox proxy, if used cautiously, has great potential to characterize different types of marine sedimentary rocks that were affected by early diagenetic processes.

6. Conclusions

The application of iron (Fe) speciation as a paleo-redox proxy − used to determine the formation conditions of hydrocarbon-derived authigenic carbonates − complements established redox proxies. In this pilot study, seep deposits from the Congo Fan, the Gulf of Mexico, and the Black Sea have been analyzed by means of Mössbauer spectroscopy and Fe contents. Authigenic carbonates from the Congo Fan revealed small isomer shifts and quadruple splitting and relatively high authigenic Fe contents, suggesting that authigenic Fe is predominantly represented by pyrite and confirming previous work that already pointed to sulfidic formation conditions. The Mössbauer parameters and authigenic Fe contents of the Gulf of Mexico seep carbonates, on the other hand, reflect different sedimentary environments with a wide range of redox conditions spanning from oxic over suboxic and anoxic, to methanogenic. Their variable Mössbauer parameters are interpreted to reflect changes in seep flux during carbonate formation. The studied Black Sea carbonates had no clear absorption peaks in the Mössbauer spectra, and revealed low contents of total Fe and

authigenic Fe, indicating that authigenic Fe minerals are scarce in the samples. These patterns are interpreted to result from suboxic conditions for a sample from 120 m water depth and sulfidic conditions for a sample from 190 m water depth, reflecting the peculiar oceanography of the Black Sea. Iron speciation in combination with the content of authigenic Fe is a useful tool to assess the wide range of past redox conditions and their variability over the life span of seeps. It will apply to other marine sediments and sedimentary rocks and will help to constrain diagenetic pathways and the environmental conditions during the formation of authigenic minerals.

References

Algeo, T., Tribovillard, N., 2009. Environmental analysis of paleoceanographic systems based on molybdenum−uranium covariation. Chem. Geol. 268, 211−225.

Bayon, G., Birot, D., Ruffine, L., Caprais, J.C., Ponzevera, E., Bollinger, C., Donval, J.P., Charlou, J.L., Voisset, M., Grimaud, S., 2011. Evidence for intense REE scavenging at cold seeps from the Niger Delta margin. Earth Planet. Sci. Lett. 312, 443−452.

Bayon, G., Dupré, S., Ponzevera, E., Etoubleau, J., Chéron, S., Pierre, C., Mascle, J., Boetius, A., De Lange, G.J., 2013. Formation of carbonate chimneys in the Mediterranean Sea linked to deep-water oxygen depletion. Nat. Geosci. 6, 755−760.

Beal, E.J., House, C.H., Orphan, V.J., 2009. Manganese- and iron-dependent marine methane oxidation. Science 325, 184−187.

Berner, R.A., 1980. Early Diagenesis − a Theoretical Approach. Princeton University Press, Princeton.

Berner, R.A., 1984. Sedimentary pyrite formation: an update. Geochim. Cosmochim. Acta 48, 605−615.

Birgel, D., Feng, D., Roberts, H.H., Peckmann, J., 2011. Changing redox conditions at cold seeps as revealed by authigenic carbonates from Alaminos Canyon, northern Gulf of Mexico. Chem. Geol. 285, 82−96.

Boetius, A., Ravenschlag, K., Schubert, C.J., Rickert, D., Widdel, F., Gieseke, A., Amann, R., Jørgensen, B.B., Witte, U., Pfannkuche, O., 2000. A marine microbial consortium apparently mediating anaerobic oxidation of methane. Nature 407, 623−626.

Boetius, A., Wenzhöfer, F., 2013. Seafloor oxygen consumption fuelled by methane from cold seeps. Nat. Geosci. 6, 725−734.

Bohrmann, G., Greinert, J., Suess, E., Torres, M., 1998. Authigenic carbonates from the Cascadia subduction zone and their relation to gas hydrate stability. Geology 26, 647−650.

Campbell, K.A., 2006. Hydrocarbon seep and hydrothermal vent paleoenvironments and paleontology: past developments and future research directions. Palaeogeogr. Palaeoclimatol. Palaeoecol. 232, 362−407.

Calvert, S.E., Karlin, R.E., 1991. Relationships between sulphur, organic carbon, and iron in the modern sediments of the Black Sea. Geochim. Cosmochim. Acta 55, 2483−2490.

Charlou, J.L., Donval, J.P., Fouquet, Y., Ondreas, H., Knoery, J., Cochonat, P., Levaché, D., Poirier, Y., Jean-Baptiste, P., Fourré, E., Chazallon, B., 2004. Physical and chemical characterization of gas hydrates and associated methane plumes in the Congo−Angola Basin. Chem. Geol. 205, 405−425.

Chen, D.F., Cathles, L.M., Roberts, H.H., 2004. The geochemical signatures of variable gas venting at gas hydrate sites. Mar. Petrol. Geol. 21, 317−326.

Chen, Z., Yan, W., Chen, M.H., Wang, S.H., Lu, J., Zhang, F., Xiang, R., Xiao, S.B., Yan, P., Gu, S.C., 2006. Discovery of seep carbonate nodules as new evidence for gas venting on the northern continental slope of South China Sea. Chin. Sci. Bull. 51, 1228−1237.

Crémière, A., Bayon, G., Ponzevera, E., Pierre, C., 2013. Paleo-environmental controls on cold seep carbonate authigenesis in the Sea of Marmara. Earth Planet. Sci. Lett. 376, 200−211.

Dewangan, P., Basavaiah, N., Badesab, F.K., Usapkar, A., Mazumdar, A., Joshi, R., Ramprasad, T., 2013. Diagenesis of magnetic minerals in a gas hydrate/cold seep

environment off the Krishna–Godavari basin, Bay of Bengal. Mar. Geol. 340, 57–70.

Feng, D., Chen, D., Roberts, H.H., 2009. Petrographic and geochemical characterization of seep carbonate from Bush Hill (GC 185) gas vent and hydrate site of the Gulf of Mexico. Mar. Petrol. Geol. 26, 1190–1198.

Feng, D., Chen, D., Peckmann, J., Bohrmann, G., 2010. Authigenic carbonates from methane seeps of the northern Congo fan: microbial formation mechanism. Mar. Petrol. Geol. 27, 748–756.

Feng, D., Lin, Z., Bian, Y., Chen, D., Peckmann, J., Bohrmann, G., Roberts, H.H., 2013. Rare earth elements of seep carbonates: Indication for redox variations and microbiological processes at modern seep sites. J. Asian Earth Sci. 65, 27–33.

Froelich, P.N., Klinkhammer, G.P., Bender, M.L., Luedtke, N.A., Heath, G.R., Cullen, D., Dauphin, P., Hammond, D., Hartman, B., Maynard, V., 1979. Early oxidation of organic matter in pelagic sediments of the eastern equatorial Atlantic: suboxic diagenesis. Geochim. Cosmochim. Acta 43, 1075–1090.

Ge, L., Jiang, S.-Y., Swennen, R., Yang, T., Yang, J.-H., Wu, N.-Y., Liu, J., Chen, D.-H., 2010. Chemical environment of cold seep carbonate formation on the northern continental slope of South China Sea: evidence from trace and rare earth element geochemistry. Mar. Geol. 277, 21–30.

González, F.J., Somoza, L., León, R., Medialdea, T., de Torres, T., Ortiz, J.E., Lunar, R., Martínez-Frías, J., Merinero, R., 2012. Ferromanganese nodules and microhardgrounds associated with the Cadiz Contourite Channel (NE Atlantic): palaeoenvironmental records of fluid venting and bottom currents. Chem. Geol. 310–311, 56–78.

Greinert, J., Bohrmann, G., Suess, E., 2001. Gas Hydrate-associated Carbonates and Methane-venting at Hydrate Ridge: Classification, Distribution, and Origin of Authigenic Lithologies. In: Geophysical Monographs 124. AGU, Washington DC, pp. 131–143.

Greinert, J., 2008. Monitoring temporal variability of bubble release at seeps: the hydroacoustic swath system GasQuant. J. Geophys. Res. 113 http://dx.doi.org/10.1029/2007JC004704.

Haas, A., Peckmann, J., Elvert, M., Sahling, H., Bohrmann, G., 2010. Patterns of carbonate authigenesis at the Kouilou pockmarks on the Congo deep-sea fan. Mar. Geol. 268, 129–136.

Han, X., Suess, E., Liebetrau, V., Eisenhauer, A., Huang, Y., 2014. Past methane release events and environmental conditions at the upper continental slope of the South China Sea: constraints by seep carbonates. Int. J. Earth Sci. 103, 1873–1887.

Hensen, C., Zabel, M., Pfeifer, K., Schwenk, T., Kasten, S., Riedinger, N., Schulz, H.D., Boetius, A., 2003. Control of sulfate pore-water profiles by sedimentary events and the significance of anaerobic oxidation of methane for the burial of sulfur in marine sediments. Geochim. Cosmochim. Acta 67, 2631–2647.

Himmler, T., Bach, W., Bohrmann, G., Peckmann, J., 2010. Rare earth elements in authigenic methane-seep carbonates as tracers for fluid composition during early diagenesis. Chem. Geol. 277, 126–136.

Hu, Y., Feng, D., Peckmann, J., Roberts, H.H., Chen, D., 2014. New insights into cerium anomalies and mechanisms of trace metal enrichment in authigenic carbonate from hydrocarbon seeps. Chem. Geol. 381, 55–66.

Joye, S., MacDonald, I., Montoya, J.P., Peccini, M., 2005. Geophysical and geochemical signatures of Gulf of Mexico seafloor brines. Biogeosciences 2, 295–309.

Joye, S.B., Samarkin, V.A., 2009. Metabolic variability in seafloor brines revealed by carbon and sulphur dynamics. Nat. Geosci. 2, 349–354.

Kim, J.-H., Torres, M.E., Haley, B.A., Kastner, M., Pohlman, J.W., Riedel, M., Lee, Y.-J., 2012. The effect of diagenesis and fluid migration on rare earth element distribution in pore fluids of the northern Cascadia accretionary margin. Chem. Geol. 291, 152–165.

Lemaitre, N., Bayon, G., Ondréas, H., Caprais, J.-C., Freslon, N., Bollinger, C., Rouget, M.-L., de Prunelé, A., Ruffine, L., Olu-Le Roy, K., Sarthou, G., 2014. Trace element behaviour at cold seeps and the potential export of dissolved iron to the ocean. Earth Planet. Sci. Lett. 404, 376–388.

Liebetrau, V., Augustin, N., Kutterolf, S., Schmidt, M., Eisenhauer, A., Garbe-Schönberg, D., Weinrebe, W., 2014. Cold-seep-driven carbonate deposits at the Central American forearc: contrasting evolution and timing in escarpment and mound settings. Int. J. Earth Sci. 103, 1845–1872.

Lyons, T.W., Berner, R.A., 1992. Carbon-sulfur-iron systematics of the uppermost deep-water sediments of the Black Sea. Chem. Geol. 99, 1–27.

Lyons, T.W., Severmann, S., 2006. A critical look at iron paleoredox proxies: new insights from modern euxinic marine basins. Geochim. Cosmochim. Acta 70, 5698–5722.

Macelloni, L., Brunner, C.A., Caruso, S., Lutken, C.B., D'Emidio, M., Lapham, L.L., 2013. Spatial distribution of seafloor bio-geological and geochemical processes as proxies of fluid flux regime and evolution of a carbonate/hydrates mound, northern Gulf of Mexico. Deep-Sea Res. I 74, 25–38.

Malone, M.J., Claypool, G., Martin, J.B., Dickens, G.R., 2002. Variable methane fluxes in shallow marine systems over geologic time: the composition and origin of pore waters and authigenic carbonates on the New Jersey shelf. Mar. Geol. 189, 175–196.

März, C., Hoffmann, J., Bleil, U., de Lange, G.J., Kasten, S., 2008. Diagenetic changes of magnetic and geochemical signals by anaerobic methane oxidation in sediments of the Zambezi deep-sea fan (SW Indian Ocean). Mar. Geol. 255, 118–130.

Medina, G., Tabares, J.A., Pérez Alcázar, G.A., Barraza, J.M., 2006. A methodology to evaluate coal ash content using siderite Mössbauer spectral area. Fuel 85, 871–873.

McLennan, S.M., 2001. Relationships between the trace element composition of sedimentary rocks and upper continental crust. Geochem. Geophys. Geosyst 2. http://dx.doi.org/10.1029/2000GC000109.

Novikova, S.A., Shnyukov, Y.F., Sokol, E.V., Kozmenko, O.A., Semenova, D.V., Kutny, V.A., 2015. A methane-derived carbonate build-up at a cold seep on the Crimean Slope, North-Western Black Sea. Mar. Geol. 363, 160–173.

Omoregie, E.O., Mastalerz, V., De Lange, G., Straub, K.L., Kappler, A., Røy, H., Stadnitskaia, A., Foucher, J.-P., Boetius, A., 2008. Biogeochemistry and community composition of iron-and sulfur-precipitating microbial mats at the Chefren mud volcano (Nile Deep Sea Fan, Eastern Mediterranean). Appl. Environ. Microbiol. 74, 3198–3215.

Owens, J.D., Lyons, T.W., Li, X., Macleod, K.G., Gordon, G., Kuypers, M.M.M., Anbar, A., Kuhnt, W., Severmann, S., 2012. Iron isotope and trace metal records of iron cycling in the proto-North Atlantic during the Cenomanian-Turonian oceanic anoxic event (OAE-2). Paleoceanography 27, PA3223.

Peckmann, J., Reimer, A., Luth, U., Luth, C., Hansen, B., Heinicke, C., Hoefs, J., Reitner, J., 2001. Methane-derived carbonates and authigenic pyrite from the northwestern Black Sea. Mar. Geol. 177, 129–150.

Peckmann, J., Thiel, V., 2004. Carbon cycling at ancient methane-seeps. Chem. Geol. 205, 443–467.

Peiffer, S., Behrends, T., Hellige, K., Larese-Casanova, P., Wan, M., Pollok, K., 2015. Pyrite formation and mineral transformation pathways upon sulfidation of ferric hydroxides depend on mineral type and sulfide concentration. Chem. Geol. 400, 44–55.

Pierre, C., Fouquet, Y., 2007. Authigenic carbonates from methane seeps of the Congo deep-sea fan. Geo-Mar. Lett. 27, 249–257.

Pierre, C., Blanc-Valleron, M.-M., Caquineau, S., März, C., Ravelo, A.C., Takahashi, K., Alvarez Zarikian, C., 2014. Mineralogical, geochemical and isotopic characterization of authigenic carbonates from the methane-bearing sediments of the Bering Sea continental margin (IODP Expedition 323, Sites U1343–U1345). Deep-Sea Res. II. http://dx.doi.org/10.1016/j.dsr2.2014.03.011.

Ram, S., Patel, K.R., Sharma, S.K., Tripathi, R.P., 1998. Distribution of iron in siderite in sub-surface sediments of Jaisalmer Basin (India) using Mössbauer spectroscopy. Fuel 77, 1507–1512.

Raiswell, R., Canfield, D.E., 2012. The iron biogeochemical cycle past and present. Geochem. Perspect. 1, 1–220.

Reitner, J., Peckmann, J., Reimer, A., Schumann, G., Thiel, V., 2005. Methane-derived carbonate build-ups and associated microbial communities at cold seeps on the lower Crimean shelf (Black Sea). Facies 51, 66–79.

Riedinger, N., Formolo, M.J., Lyons, T.W., Henkel, S., Beck, A., Kasten, S., 2014. An inorganic geochemical argument for coupled anaerobic oxidation of methane and iron reduction in marine sediments. Geobiology 12, 172–181.

Roberts, H.H., Aharon, P., 1994. Hydrocarbon-derived carbonate buildups of the northern Gulf of Mexico continental slope: a review of submersible investigations. Geo Mar. Lett. 14, 135–148.

Rongemaille, E., Bayon, G., Pierre, C., Bollinger, C., Chu, N.C., Fouquet, Y., Riboulot, V., Voisset, M., 2011. Rare earth elements in cold seep carbonates from the Niger delta. Chem. Geol. 286, 196–206.

Severmann, S., McManus, J., Berelson, W.M., Hammond, D.E., 2010. The continental shelf benthic iron flux and its isotope composition. Geochim. Cosmochim. Acta 74, 3984–4004.

Scholz, F., McManus, J., Mix, A.C., Hensen, C., Schneider, R.R., 2014a. The impact of ocean deoxygenation on iron release from continental margin sediments. Nat. Geosci. 7, 433–437.

Scholz, F., Severmann, S., McManus, J., Hensen, C., 2014b. Beyond the Black Sea paradigm: the sedimentary fingerprint of an open-marine iron shuttle. Geochim. Cosmochim. Acta 127, 368–380.

Schneider von Deimling, J., Rehder, G., Greinert, J., McGinnnis, D.F., Boetius, A., Linke, P., 2011. Quantification of seep-related methane gas emissions at Tommeliten, North Sea. Cont. Shelf Res. 31, 867–878.

Sivan, O., Antler, G., Turchyn, A.V., Marlow, J.J., Orphan, V.J., 2014. Iron oxides stimulate sulfate-driven anaerobic methane oxidation in seeps. Proc. Natl. Acad. Sci. 111, E4139–E4147.

Solomon, E.A., Kastner, M., Jannasch, H., Robertson, G., Weinstein, Y., 2008. Dynamic fluid flow and chemical fluxes associated with a seafloor gas hydrate deposit on the northern Gulf of Mexico slope. Earth Planet. Sci. Lett. 270, 95–105.

Suess, E., 2014. Marine cold seeps and their manifestations: geological control, biogeochemical criteria and environmental conditions. Int. J. Earth Sci. 103, 1889–1916.

Sun, Z., Wei, H., Zhang, X., Shang, L., Yin, X., Sun, Y., Xu, L., Huang, W., Zhang, X., 2015. A unique Fe-rich carbonate chimney associated with cold seeps in the Northern Okinawa Trough, East China Sea. Deep Sea Res. I 95, 37–53.

Thomson, J., Higgs, N.C., Croudace, I.W., Colley, S., Hydes, D.J., 1993. Redox zonation of elements at an oxic/post-oxic boundary in deep-sea sediments. Geochim. Cosmochim. Acta 57, 579–595.

Tribovillard, N., Algeo, T.J., Lyons, T., Riboulleau, A., 2006. Trace metals as paleoredox and paleoproductivity proxies: an update. Chem. Geol. 232, 12–32.

Tribovillard, N., Hatem, E., Averbuch, O., Barbecot, F., Bout-Roumazeilles, V., Trentesaux, A., 2015. Iron availability as a dominant control on the primary composition and diagenetic overprint of organic-matter-rich rocks. Chem. Geol. 401, 67–82.

Tryon, M.D., Brown, K.M., Torres, M.E., Tréhu, A.M., McManus, J., Collier, R.W., 1999. Measurements of transience and downward fluid flow near episodic methane gas vents, Hydrate Ridge, Cascadia. Geology 27, 1075–1078.

Tryon, M.D., Brown, K.M., 2004. Fluid and chemical cycling at Bush Hill: Implications for gas-and hydrate-rich environments. Geochem. Geophys. Geosyst. 5, 1–7.

Vandenberghe, R., De Grave, E., 2013. Application of mössbauer spectroscopy in Earth Sciences. In: Yoshida, Y., Langouche, G. (Eds.), Mössbauer Spectroscopy. Springer Berlin Heidelberg, pp. 91—185.

Zachara, J.M., Kukkadapu, R.K., Gassman, P.L., Dohnalkova, A., Fredrickson, J.K., Anderson, T., 2004. Biogeochemical transformation of Fe minerals in a petroleum-contaminated aquifer. Geochim. Cosmochim. Acta 68, 1791—1805.

Zheng, G., Lang, Y., Takano, B., Matsuo, M., Kuno, A., Tsushima, H., 2002. Iron specia- tion of sliding mud in Toyama Prefecture, Japan. J. Asian Earth Sci. 20, 955—963.

Zheng, G., Fu, B., Takahashi, Y., Kuno, A., Matsuo, M., Zhang, J., 2010. Chemical speciation of redox sensitive elements during hydrocarbon leaching in the Junggar Basin, Northwest China. J. Asian Earth Sci. 39, 713—723.

Zhang, Z., Zheng, G., Shozugawa, K., Matsuo, M., Zhao, Y., 2013. Iron and sulfur speciation in some sedimentary-transformation-type of lead—zinc deposits in West Kunlun lead—zinc ore deposit zone, Northwest China. J. Radioanal. Nucl. Chem. 297, 83—90.

Zhang, M., Konishi, H., Xu, H.F., Sun, X.M., Lu, H.F., Wu, D.D., Wu, N.Y., 2014. Morphology and formation mechanism of pyrite induced by the anaerobic oxidation of methane from the continental slope of the NE South China Sea. J. Asian Earth Sci. 92, 293—301.